Scalable Electric Vehicle Charging Protocols

Liang Zhang, *Student Member, IEEE*, Vassilis Kekatos, *Member, IEEE*, and Georgios B. Giannakis, *Fellow, IEEE*

***Abstract*—Although electric vehicles are considered a viable solution to reduce greenhouse gas emissions, their uncoordinated charging could have adverse effects on power system operation. Nevertheless, the task of optimal electric vehicle charging scales unfavorably with the fleet size and the number of control periods, especially when distribution grid limitations are enforced. To this end, vehicle charging is first tackled using the recently revived Frank–Wolfe method. The novel decentralized charging protocol has minimal computational requirements from vehicle controllers, enjoys provable acceleration over existing alternatives, enhances the security of the pricing mechanism against data attacks, and protects user privacy. To comply with voltage limits, a network-constrained EV charging problem is subsequently formulated. Leveraging a linearized model for unbalanced distribution grids, the goal is to minimize the power supply cost while respecting critical voltage regulation and substation capacity limitations. Optimizing variables across grid nodes is accomplished by exchanging information only between neighboring buses via the alternating direction method of multipliers. Numerical tests corroborate the optimality and efficiency of the novel schemes.**

***Index Terms*—Alternating direction method of multipliers (ADMM), Frank–Wolfe algorithm, linearized distribution flow model.**

I. Introduction

ELECTRIC vehicles (EVs) have received significant attention from the automotive industry and the government due to their capacity to reduce greenhouse gas emissions and mitigate oil dependency. Nevertheless, the overall load profile will be greatly affected with increasing numbers of EVs. Uncoordinated charging of even a 10% penetration of EV loads will notably affect power system operation, giving rise to voltage magnitude fluctuations and unacceptable load peaks [1]. On the other hand, with proper coordination, EV loads can be controlled to minimize charging costs or perform valley-filling tasks relying on advanced power electronics.

Different charging control schemes have been proposed. A centralized scheduling scheme to minimize total charging costs based on the time-of-use price has been devised in [2]. However, new load peaks may arise during low-price (also termed valley) periods. In [3], vehicle plug-in times are decided using random numbers, hence neglecting the specific charging requests of individual EV users. Charging rates have been also optimized in a centralized manner to facilitate voltage regulation [1], yet the number of control variables scales unfavorably with the number of vehicles.

Decentralized control strategies not only offer computational savings, but they oftentimes enhance the privacy of vehicle users since they do not require the charging requests of EVs to be uploaded to the control center. Decentralized charging protocols based on congestion pricing schemes similar to those used in Internet Protocol networks can be found in [4]; nevertheless, their optimality is not guaranteed. Presuming identical energy requests and plug-in/-out times for all vehicles, a game-theoretic charging scheme attaining a Nash equilibrium has been developed in [5]. Iterative schemes based on Lagrangian relaxation are suggested in [6], [7], while [8] builds on the alternating direction method of multipliers (ADMM). Distribution locational marginal prices are leveraged to coordinate vehicle charging in [9]. Reference [10] proves a feasible valley-filling charging profile to be optimal for any convex cost, and it develops a decentralized protocol based on projected gradient descent (PGD). A multi-agent based EV charging scheme is devised in [11]. The spatial coupling of EV charging decisions due to transformer capacity limits is tackled in [12] via a combination of the ADMM and PGD. Upon neglecting total charging requirements, dual decomposition and projected subgradient are applied to real-time decentralized EV charging in [13]. The online charging scheme of [14] minimizes the regret in charging cost, but only in the long term.

Vehicle charging under distribution grid limitations has been studied too. Centralized EV scheduling is studied under different linear models for multiphase networks in [15] and [16]. The objective function is confined to be linear and the optimal solution is found using generic commercial solvers without exploiting the problem structure. A method for heuristically checking network constraint violations after vehicles have been scheduled is reported in [17]. Presuming at most one EV per bus, management under balanced network constraints has been tackled using a water-filling algorithm [18].

The optimal vehicle charging problem considered here can be rigorously stated as follows. Given charging requests from EVs across time, a utility company schedules their charging to minimize certain cost function, e.g., the power supply cost or the load variance. The latter is equivalent to the so termed the *valley-filling* task. Depending on whether grid specifications are taken into account, two charging scenarios can be recognized. The first scenario ignores any grid-related constraints. Such a scenario arises for example when the EV load is relatively low

Manuscript received January 17, 2016; revised May 5, 2016; accepted June 18, 2016. Date of publication June 21, 2016; date of current version February 16, 2017. This work was supported by NSF under Grants 1423316, 1442686, 1508993, and 1509040. Paper no. TPWRS-00102-2016.

L. Zhang and G. B. Giannakis are with the Digital Technology Center and the Department of Electrical & Computer Engineering, University of Minnesota, Minneapolis, MN 55455 USA (e-mail: zhan3523@umn.edu; georgios@umn.edu).

V. Kekatos is with the Bradley Department of Electrical & Computer Engineering, Virginia Tech, Blacksburg, VA 24061 USA (e-mail: kekatos@vt.edu).

Color versions of one or more of the figures in this paper are available online at http://ieeexplore.ieee.org.

Digital Object Identifier 10.1109/TPWRS.2016.2582903

and is not expected to incur voltage or feeder violations; see the valley-filling task in [10]. In this first scenario, vehicle charging may be alternatively performed by a charging station or a load aggregator to minimize its power supply cost. Under the second scenario, EV penetration is high, and thus, voltage regulation and feeder limitations must be enforced by the utility. Apparently, the first scenario constitutes a relaxation of the second scenario of *network-constrained* vehicle charging. Thus, protocols for the first scenario will be used as building modules for the second one.

Our contribution is two-fold. First, a decentralized charging method based on the Frank–Wolf algorithm is developed (see Section II). Different from existing schemes, the novel protocol requires minimal requirements from the vehicle charging controllers and involves privacy-preserving updates. Numerical tests demonstrate that the closed-form low-complexity updates yield significant convergence improvement over existing alternatives (see Section V-A). Secondly, building on an approximate distribution grid model, network-constrained EV charging is formulated as a convex quadratic program (see Section III), and tackled using a decentralized scheme based on ADMM (see Section IV). Compared to existing centralized schemes, the decentralized protocol requires communication only between neighbors and preserves the privacy of EV owners. Numerical tests on the unbalanced IEEE 123-bus feeder corroborate the optimality of the proposed charging protocol (see Section V-B).

Regarding *notation*, column vectors (matrices) are denoted by lower- (upper-) case boldface letters, except for power flow vectors $(\mathbf{P}, \mathbf{Q}, \mathbf{S})$. Sets are represented using calligraphic symbols, and $|\mathcal{S}|$ is the cardinality of $\mathcal{S}$. Symbol $^\top$ stands for transposition; while $\mathbf{0}$, $\mathbf{1}$, and $\mathbf{e}_n$, denote respectively the all-zeros, all-ones, and the nth canonical vectors. Operator $\mathrm{diag}(\mathbf{x})$ defines a diagonal matrix having $\mathbf{x}$ on its diagonal, and $\mathrm{Re}(z)$ returns the real part of complex number z.

II. Optimal Vehicle Charging

This section studies EV charging without network constraints. Under this scenario, the utility company, a load aggregator, or a charging station would like to coordinate EVs to minimize the power supply cost or for valley-filling purposes. Upon formulating the problem, an optimal charging scheme is developed and contrasted to state-of-the-art alternatives.

A. EV Charging Model

An EV scheduler coordinates the charging of M EVs over a period of T consecutive time slots comprising the set $\mathcal{T} := \{1, \ldots, T\}$. The time slot duration ΔT can range from minutes to an hour, depending on charging specifications, the granularity of load forecasts, as well as communication and computation capabilities. Let $e_m(t)$ denote the energy charge for vehicle m at time t with $m = 1, \ldots, M$, and $t \in \mathcal{T}$. Given that operational slots have equal duration, the terms power and energy will be used interchangeably. The charge $e_m(t)$ can range from zero to its maximum value $\bar{e}_m(t)$. Apparently, a vehicle can be charged only when it is connected to the grid. If $\mathcal{T}_m \subseteq \mathcal{T}$ is the set of time slots that vehicle m is connected to the grid (not necessarily consecutive), then for all $t \in \mathcal{T}$

$$\bar{e}_m(t) = \begin{cases} \bar{e}_m \ , & t \in \mathcal{T}_m \\ 0 \quad , & \text{otherwise} \end{cases}$$

where $\bar{e}_m$ is the maximum charging rate determined by the battery of vehicle m. Let $\mathbf{e}_m := [e_m(1) \ \cdots \ e_m(T)]^\top$ be the charging profile for EV m. Profile $\mathbf{e}_m$ should belong to the compact and convex set

$$\mathcal{E}_m := \{\mathbf{e}_m : \mathbf{e}_m^\top \mathbf{1} = R_m, \ 0 \leq e_m(t) \leq \bar{e}_m(t) \ \forall \ t \in \mathcal{T}\} \quad (1)$$

where R_m is the total energy needed by EV m. The latter depends on the initial state of charge, the desired state of charge, and the efficiency of the battery.

Through coordinated charging of EVs, various objectives can be achieved, such as minimizing charging costs or valley-filling. Optimal EV charging can be posed as the optimization problem [10]

$$\min_{\{\mathbf{e}_m\}_{m=1}^M} \quad C(\{\mathbf{e}_m\}) := \sum_{t=1}^{T} C_t \left(d(t) + \sum_{m=1}^{M} e_m(t) \right) \quad (2)$$

$$\text{s.to} \ \ \mathbf{e}_m \in \mathcal{E}_m, \ \forall \ m = 1, \ldots, M$$

where the energy costs $C_t(\cdot) : \mathbb{R} \to \mathbb{R}$ are assumed convex and differentiable. For charging cost minimization, $\{C_t\}_{t=1}^T$ can be linear or quadratic [2]; while $C_t(x) = x^2/2$ for all t when it comes to the valley-filling task. Parameters $\{d(t)\}_{t=1}^T$ capture the base load for the EV scheduler, which is assumed inelastic and known in advance. The network-constrained EV charging is postponed for Section III, wherein problem (2) turns out to be a building module. To facilitate scheduling, each EV controller is capable of two-way communication and of executing simple computation tasks. Before the beginning of the charging horizon $\mathcal{T}$, vehicle controllers submit their charging requests $\{(\mathcal{T}_m, R_m)\}$ to the charging station controller. Protocols for efficiently solving (2) are presented next.

B. Scalable Charging Protocol

Observe that the total number of variables involved in (2) is MT. Therefore, although (2) is a convex problem, solving it is a non-trivial task, particularly for large EV fleets and/or decreasing control intervals ΔT. To derive a scalable solver, the Frank–Wolfe method is deployed next [19]. Also known as conditional gradient algorithm, the Frank–Wolfe method aims at solving the generic problem

$$\mathbf{y}^* \in \arg\min_{\mathbf{y} \in \mathcal{Y}} \ f(\mathbf{y}) \quad (3)$$

where f is a differentiable convex function, and $\mathcal{Y}$ is a compact convex set. The method selects an initial $\mathbf{y}^0$ arbitrarily, and iterates between the updates for $k = 0, 1, \ldots,$ as

$$\mathbf{r}^k \in \arg\min_{\mathbf{r} \in \mathcal{Y}} \ \mathbf{r}^\top \nabla f(\mathbf{y}^k) \quad (4a)$$

$$\mathbf{y}^{k+1} := \mathbf{y}^k + \eta_k (\mathbf{r}^k - \mathbf{y}^k) \quad (4b)$$

with $\eta_k := 2/(k+2)$. Step (4a) finds $\mathbf{r}^k$ such that $(\mathbf{r}^k - \mathbf{y}^k)$ is a feasible descent direction for the first-order approximation

of the cost in (3). Step (4b) updates $\mathbf{y}^k$ towards that direction after scaling it with the diminishing step size η_k. The updated $\{\mathbf{y}^{k+1}\}$ is always feasible, since $\eta^0 = 1,\ \mathbf{y}^1 = \mathbf{r}^0 \in \mathcal{Y}$, and for $k \geq 1$, $\mathbf{y}^{k+1}$ is computed as the convex combination of $\mathbf{y}^k \in \mathcal{Y}$ and $\mathbf{r}^k \in \mathcal{Y}$.

Granted that (2) entails a differentiable cost and a compact feasible set; it is amenable to Frank–Wolfe iterations. In the first Frank–Wolfe step, the gradient of the cost in (2) with respect to $\{\mathbf{e}_m\}_{m=1}^M$ must be obtained. Critically, due to the problem structure, the per-vehicle partial gradients of the cost are all *identical* to

$$\nabla_{\mathbf{e}_m} C(\{\mathbf{e}_m\}) = \mathbf{g}, \quad m = 1, \ldots, M.$$

It can be readily checked that the tth entry of the common partial gradient $\mathbf{g} \in \mathbb{R}^T$ evaluated at $\{\mathbf{e}_m^k\}$ is

$$g^k(t) = \nabla_{e_m^k(t)} C_t \left(d(t) + \sum_{m=1}^{M} e_m^k(t) \right), \ t = 1, \ldots, T. \quad (5)$$

Applying (4a) to the problem at hand requires solving

$$\{\mathbf{r}_m^k\}_{m=1}^M \in \arg \min_{\{\mathbf{r}_m \in \mathcal{E}_m\}_{m=1}^M} \sum_{m=1}^{M} \mathbf{r}_m^\top \mathbf{g}^k \quad (6)$$

which is separable across vehicles. Thus, given $\mathbf{g}^k$, vehicle m needs to solve the linear program

$$\mathbf{r}_m^k \in \arg \min_{\mathbf{r}_m \in \mathcal{E}_m} \mathbf{r}_m^\top \mathbf{g}^k. \quad (7)$$

Problem (7) involves a linear cost minimized over a weighted budget and box constraints. The key observation here is that due to the aforementioned structure, problem (7) can be solved by a simple sorting algorithm [20, Chap. 4]: The entries of $\mathbf{g}^k$ are first sorted in increasing order as

$$g^k(t_1^k) \leq g^k(t_2^k) \leq \cdots \leq g^k(t_T^k). \quad (8)$$

Since the problems in (7) share vector $\mathbf{g}^k$ for all m, the sorting operation is performed only once by the charging station. Then, for vehicle m, we need to find the index J_m^k for which

$$\sum_{j=1}^{J_m^k} \bar{e}_m(t_j^k) \leq R_m \text{ and } \sum_{j=1}^{J_m^k+1} \bar{e}_m(t_j^k) > R_m. \quad (9)$$

Subsequently, the entries of the minimizer $\mathbf{r}_m^k$ of (7) can be computed per vehicle m as

$$r_m^k(t_j^k) = \begin{cases} \bar{e}_m(t_j^k) & , j = 1, \ldots, J_m^k - 1 \\ R_m - \sum_{j=1}^{J_m^k - 1} \bar{e}_m(t_j^k) & , j = J_m^k \\ 0 & , j = J_m^k + 1, \ldots, T \end{cases}. \quad (10)$$

The solution in (10) simply selects the maximum possible charge during the cheapest time slots in a greedy fashion. Interestingly, finding $\mathbf{r}_m^k$ from (10) requires knowing solely the rank order (smallest to largest) rather than the actual entries of the gradient vector $\mathbf{g}^k$.

The second Frank–Wolfe step updates the charging profiles via the convex combinations

$$\mathbf{e}_m^{k+1} = (1 - \eta_k)\mathbf{e}_m^k + \eta_k \mathbf{r}_m^k \quad (11)$$

Algorithm 1: Decentralized EV scheduling.

1: Initialize $\mathbf{e}_m^0 = \mathbf{0}$ for $m = 1, \ldots, M$.
2: **for** $k = 0, 1, \ldots$ **do**
3: EV scheduler calculates $\mathbf{g}^k$ from (5).
4: EV scheduler broadcasts $\mathbf{g}^k$ entry ranking to EVs.
5: Vehicles update $\{\mathbf{e}_m^k\}_{m=1}^M$ via (9)–(11).
6: Profile sums $\sum_{m=1}^M \mathbf{e}_m^k$ sent to control center.
7: **end for**

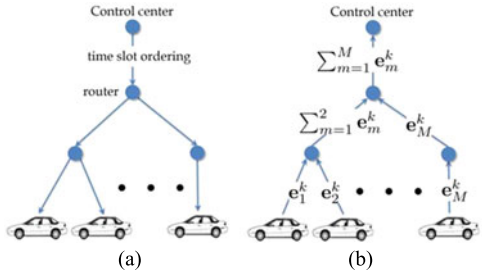

Fig. 1. Information exchange for Algorithm 1 at iteration k. (a) Control center broadcasts time slot pricing ordering (from cheapest to most expensive) to EV controllers. (b) Summations of charging profiles are transmitted to charging control center.

for all vehicles $m = 1, \ldots, M$.

To practically implement (5)–(11) during iteration k, the charging control center evaluates the cost gradients $\{g^k(t)\}_{t \in \mathcal{T}}$ defined in (5), and sorts them to determine the time slot ordering $\{t_1^k, t_2^k, \ldots, t_T^k\}$. This sorting operation can be performed using for example the Merge-Sort algorithm in $\mathcal{O}(T \log T)$ operations [21]. The price ordering of time slots is subsequently broadcast to all EV controllers as shown in Fig. 1(a). Based on its charging needs $\mathcal{E}_m$, the mth EV controller first finds $\mathbf{r}_m^k$ from (9), (10) in $\mathcal{O}(T)$. It then updates its charging profile $\mathbf{e}_m^{k+1}$ using (11) in $\mathcal{O}(T)$. Note that operations (9)–(11) can be performed in parallel over the M EV controllers. The updated charging profiles $\{\mathbf{e}_m^{k+1}\}_{m=1}^M$ are communicated back to the charging center, where upon adding the base load $\{d(t)\}$, the center computes the updated cost gradient $\mathbf{g}^{t+1}$, and iterations proceed as tabulated in Algorithm 1. The developed solver converges to optimal charging profiles $\{\mathbf{e}_m^*\}$ at the rate [19]

$$C(\{\mathbf{e}_m^k\}) - C(\{\mathbf{e}_m^*\}) \leq \mathcal{O}\left(\frac{1}{k}\right). \quad (12)$$

Algorithm 1 not only exhibits provable convergence and low computational cost (namely $\mathcal{O}(T \log T)$ operations) per iteration. It further enjoys two additional advantages. First, the charging center does not require knowing the individual charging profiles $\{\mathbf{e}_m^k\}$, since their summation $\sum_{m=1}^M \mathbf{e}_m^k$ suffices for finding the gradient vector $\mathbf{g}^k$. In an effort to preserve the privacy of EV users, a simple communication protocol can be designed. Information flow can be arranged over a tree graph rooted at the charging center, and vehicle controllers constitute the remaining tree nodes. Each node receives aggregate charging profiles from its downstream nodes, adds them up to its own profile, and forwards the updated aggregate charging profile to its parent node. As a second feature, vehicle controllers do not need to know the precise value of the cost gradient vector

$\mathbf{g}^k$, but only the ordering of its entries (current price ordering of time slots). This algorithmic feature lightens the communication load from the charging center to the vehicles, and enhances resiliency to price manipulations and data attacks to the solving scheme.

C. Comparison With Previous Work

The optimal EV charging of (2) has been previously studied in [10], where a PGD solver was developed. Interpreted here as a projected gradient algorithm applied to minimize the non-strongly convex cost in (2), the PGD method exhibits a convergence rate of $\mathcal{O}(\frac{1}{k})$ [22]. At iteration k of the PGD method, controller m solves in parallel

$$\mathbf{e}_m^{k+1} := \arg \min_{\mathbf{e}_m \in \mathcal{E}_m} \|\mathbf{e}_m - (\mathbf{e}_m^k - \eta_k' \mathbf{g}^k)\|_2^2 \tag{13}$$

for a step size $\eta_k' > 0$. In other words, every EV controller projects vector $(\mathbf{e}_m^k - \eta_k' \mathbf{g}^k)$ onto the simplex $\mathcal{E}_m$, which is a non-trivial task.

On the other hand, each iteration of Algorithm 1 involves closed-form updates, offering high computational efficiency and posing affordable hardware requirements on EV controllers. Although both Algorithm 1 and the PGD solver are decentralized schemes with convergence rate $\mathcal{O}(\frac{1}{k})$, the overall computation time for the former is significantly lower due to its simpler per-iteration updates: The numerical tests in Section V-A demonstrate that Alg. 1 provides a 100 times speed-up advantage over the PGD solver and the centralized solver SeDuMi. The SeDuMi solver would be a viable option for tackling (2) in a centralized manner after collecting all charging needs $\{(R_m, \mathcal{E}_m)\}$ at the charging center.

D. Real-Time Scheduling

Algorithm 1 requires all EVs to negotiate with the scheduler at the beginning of the control horizon. This presumption can be satisfied for charging coordination in a residential area where EVs are primarily used for commuting. Nevertheless, there are cases where EVs arrive randomly at a charging station. Then, not all charging needs are known at the beginning of the control horizon; instead, they are revealed to the scheduler in an online manner. To address random EV arrivals, a real-time implementation of Alg. 1 is pursued next.

At time t, the scheduler negotiates only with the plugged-in EVs comprising the set $\mathcal{M}^t$, while current EV energy demands are denoted by $\{R_m^t\}_{m \in \mathcal{M}^t}$. Ignoring future vehicle arrivals and their energy needs, charging of the EVs in the set $\mathcal{M}^t$ from time t till the latest departure time is coordinated by Alg. 1. After running Alg. 1, the vehicles in $\mathcal{M}^t$ are charged by $\{e_m(t)\}_{m \in \mathcal{M}^t}$ during the current time slot t, and their charging demands are updated as

$$R_m^{t+1} = R_m^t - e_m(t) \text{ for all } m \in \mathcal{M}^t. \tag{14}$$

The scheduler proceeds to time $t+1$, newly arrived vehicles are taken into account, and the process is repeated.

The overall real-time vehicle scheduling scheme is summarized as Alg. 2. Algorithm 2 essentially runs Alg. 1 only for the EVs plugged-in at every time slot. Even though no optimality can be guaranteed for Alg. 2, this scheme aims greedily for the best instantaneous charging solution while always maintaining feasibility. A related algorithm based on the PGD method is devised in [10].

Algorithm 2: Real-time decentralized EV scheduling.

```
Initialize e_m^0 = 0 for all m ∈ M^0.
for t = 1, 2, ..., T do
    Scheduler negotiates with EVs in M^t.
    for k = 0, 1, ..., do
        EV scheduler calculates and broadcasts g^k.
        Vehicles update {e_m^k}_{m∈M^t} via (9)–(11).
        Profile sums Σ_{m∈M^t} e_m^k sent to control center.
    end for
    Energy needs {R_m^t}_{m∈M^t} are updated from (14).
end for
```

III. Network-Constrained EV Scheduling

The charging scheme of Section II applies to scenarios where EV charging can be transparently supported by the underlying grid. If higher levels of EV load incur voltage magnitude or feeder capacity violations, the underlying power distribution grid needs to be taken into account. In this context, upon reviewing an approximate model for unbalanced distribution grids, this section formulates a network-constrained vehicle charging task, while a decentralized solver scalable to the number of buses and EVs is developed in Section IV.

A. Modeling Unbalanced Distribution Grids

EVs are connected to a distribution feeder comprising $N+1$ buses indicated by $n \in \mathcal{N} := \{0, 1, \ldots, N\}$, and phases indexed by $\phi \in \{a, b, c, \}$. Let $\mathcal{M}_{n,\phi}$ represent the set of vehicles located on phase ϕ of bus n, and $M_{n,\phi} := |\mathcal{M}_{n,\phi}|$. The distribution grid is assumed to be functionally radial with the substation bus numbered by $n = 0$. Every non-feeder bus $n \in \mathcal{N}^+$ with $\mathcal{N}^+ := \mathcal{N} \setminus \{0\}$ has a unique parent bus indexed by π_n. The distribution line connecting bus π_n with bus n is denoted by n. For bus n, let also $\mathcal{C}_n$ denote the set of its children buses, and $\mathcal{P}_n \subseteq \{a, b, c\}$ the set of its phases.

To enforce distribution network and voltage regulation limitations, the underlying physical system is taken into account. For that purpose, the distribution grid can be captured either by the full ac power flow model or the linearized power flow model proposed in [23]. The former becomes tractable under appropriate conditions using convex relaxations [23], [24]. However, counterexamples indicate that convex relaxations are not always successful and they can increase the computational requirements. On the other hand, several numerical tests verify that the linearized model constitutes a good approximation: the error in voltage magnitudes is within the order of 10^{-3} for various power flow studies [23], [25]. Although the linearized grid model is adopted here to simplify calculations, extending our charging protocol to the full ac model is straightforward.

Let $\mathbf{v}_n$, $\mathbf{p}_n$, and $\mathbf{q}_n$ be respectively the 3-dimensional vectors of squared voltage magnitudes and (re)active power injections for all phases of bus n. For line $n \in \mathcal{N}$, let $\mathbf{Z}_n = \mathbf{Z}_n^\top \in \mathbb{R}^{3\times 3}$ be the related phase impedance matrix, and $\mathbf{P}_n$ and $\mathbf{Q}_n$ be the vectors of (re)active power flows on all phases of line n. If line losses are relatively small and voltages are roughly balanced, the linearized multi-phase power flow model reads [23], [25]

$$\mathbf{p}_n = \sum_{k\in\mathcal{C}_n} \mathbf{P}_k - \mathbf{P}_n \tag{15a}$$

$$\mathbf{q}_n = \sum_{k\in\mathcal{C}_n} \mathbf{Q}_k - \mathbf{Q}_n \tag{15b}$$

$$\mathbf{v}_{\pi_n} - \mathbf{v}_n = \mathrm{Re}\left\{\bar{\mathbf{Z}}_n(\mathbf{P}_n + j\mathbf{Q}_n)\right\} \tag{15c}$$

where $\bar{\mathbf{Z}}_n := 2\mathrm{diag}(\boldsymbol{\alpha})\mathbf{Z}_n^*\mathrm{diag}(\boldsymbol{\alpha}^*)$; $\boldsymbol{\alpha} := [1\, \alpha\, \alpha^2]^\top$; $\alpha = e^{-j\frac{2\pi}{3}}$; and * denotes complex conjugation. When not all phases are present, power injection and flow vectors and phase impedance matrices are zero-padded. For (15c) to hold, the entries of $\mathbf{v}_n$ associated with non-existing phases are arbitrarily set to the corresponding entries of $\mathbf{v}_{\pi_n}$.

B. Network-Constrained EV Scheduling

To facilitate network-constrained EV scheduling, the base active and reactive power loads $\{(\mathbf{d}_n(t), \mathbf{q}_n^d(t))\}$ for all n and t need to be predicted in advance. Active power loads $\mathbf{p}_n^d(t)$ consist of two parts: the base loads $\mathbf{d}_n(t)$ and the EV charging load. If $p_{n,\phi}^d(t)$ and $d_{n,\phi}(t)$ are respectively the total active load and the base load on phase ϕ of bus n, it holds that $p_{n,\phi}^d(t) = d_{n,\phi}(t) + \sum_{m\in\mathcal{M}_{n,\phi}} e_m(t)$. The cost $f_0(\mathbf{P}_0(t))$ of power supply from the main grid is convex and known in advance. Variables $\mathbf{p}_n^g(t)$ capture possible dispatchable generation distributed across the feeder, and $f_n^g(\mathbf{p}_n^g(t))$ is the associated convex quadratic cost for all $n \in \mathcal{N}$ and $t \in \mathcal{T}$.

To capture operational constraints, the following limits are introduced. Let $(\underline{p}_{n,\phi}^g, \underline{q}_{n,\phi}^g)$ be the lower, and $(\bar{p}_{n,\phi}^g, \bar{q}_{n,\phi}^g)$ the upper limits for distributed generation at phase $\phi \in \mathcal{P}_n$ of bus n. Define also $(\underline{v}_{n,\phi}, \bar{v}_{n,\phi})$ as the limits of squared voltage magnitudes at phase $\phi \in \mathcal{P}_n$ of bus n, $\bar{S}_n$ as the apparent power flow limits on line n, and $\bar{S}_f$ as the rated capacity of the feeder transformer. The utility company aims to minimize the total operation cost by coordinating vehicle charging and generation dispatch, while respecting charging and operational limitations. The pertinent network-constrained EV scheduling task can be posed as:

$$\min \sum_{t\in\mathcal{T}} \left[f_0(\mathbf{P}_0(t)) + \sum_{n\in\mathcal{N}} f_n^g\left(\mathbf{p}_n^g(t)\right) \right] \tag{16a}$$

$$\text{over } \{\mathbf{p}_n^g(t), \mathbf{q}_n^g(t), \mathbf{P}_n(t), \mathbf{Q}_n(t), \mathbf{v}_n(t)\}_{n\in\mathcal{N}, t\in\mathcal{T}}, \{\mathbf{e}_m\}$$

$$\text{s.to } \mathbf{p}_n^g(t) - \mathbf{p}_n^d(t) = \sum_{k\in\mathcal{C}_n} \mathbf{P}_k(t) - \mathbf{P}_n(t),\ \forall\, n, t \tag{16b}$$

$$\mathbf{q}_n^g(t) - \mathbf{q}_n^d(t) = \sum_{k\in\mathcal{C}_n} \mathbf{Q}_k(t) - \mathbf{Q}_n(t),\ \forall\, n, t \tag{16c}$$

$$\mathbf{v}_{\pi_n}(t) - \mathbf{v}_n(t) = \mathrm{Re}\{\bar{\mathbf{Z}}_n(\mathbf{P}_n(t) + j\mathbf{Q}_n(t))\}, \forall n, t \tag{16d}$$

$$\underline{p}_{n,\phi}^g \le p_{n,\phi}^g(t) \le \bar{p}_{n,\phi}^g,\ \forall\, \phi \in \mathcal{P}_n, n, t \tag{16e}$$

$$\underline{q}_{n,\phi}^g \le q_{n,\phi}^g(t) \le \bar{q}_{n,\phi}^g,\ \forall\, \phi \in \mathcal{P}_n, n, t \tag{16f}$$

$$\underline{v}_n \le v_{n,\phi}(t) \le \bar{v}_n,\ \forall\, \phi \in \mathcal{P}_n, n, t \tag{16g}$$

$$P_{n,\phi}^2(t) + Q_{n,\phi}^2(t) \le \bar{S}_n^2,\ \forall\, \phi \in \mathcal{P}_n, n \in \mathcal{N}^+, t \tag{16h}$$

$$p_{n,\phi}^d(t) = d_{n,\phi}(t) + \sum_{m\in\mathcal{M}_{n,\phi}} e_m(t), \forall\, \phi \in \mathcal{P}_n, n, t \tag{16i}$$

$$\mathbf{e}_m \in \mathcal{E}_m,\ \forall\, m \tag{16j}$$

$$(\mathbf{1}^\top\mathbf{P}_0(t))^2 + (\mathbf{1}^\top\mathbf{Q}_0(t))^2 \le \bar{S}_f^2,\ \forall\, t. \tag{16k}$$

Constraints (16b)–(16d) originate from the power flow model; constraints (16e)–(16f) enforce generation limits; voltage regulation is guaranteed via (16g); apparent power flows are upper bounded by (16h); the equalities in (16i) define demands across phases and buses; constraint (16j) is related to the per-vehicle charging profile; and (16k) results from the capacity limit of the feeder transformer.

The cost functions and all the constraints apart from the EV charging constraint in (16j) are *separable across time*. The capacity limit in (16k) couples flows across phases, while the voltage regulation constraints in (16d) and (16g) couple variables across buses and phases. For linear and convex quadratic costs, problem (16) can be reformulated as a standard quadratically-constrained quadratic program and tackled by standard solvers in a centralized manner. Nonetheless, for increasing grid sizes, longer time horizons $\mathcal{T}$, and/or shorter control periods, tackling (16) could be challenging: Phase ϕ of bus n involves five variables $(v_{n,\phi}, p_{n,\phi}, q_{n,\phi}, P_{n,\phi}, Q_{n,\phi})$. Assuming for simplicity that every bus carries all three phases results in a total of $(15N + M)T$ variables. In addition, private information on a per-vehicle basis needs to be collected and processed by the utility. These considerations motivate well the scalable (both in space and time) and the privacy-preserving scheme for solving (16) that is pursued next.

IV. Distributed Optimal Charging Protocol

This section delineates an ADMM-based method for decomposing (16) into smaller subproblems. Notably, each subproblem either enjoys a closed-form solution or it can be tackled efficiently by Alg. 1. As a brief review, ADMM solves problems of the form [26]

$$\min_{\mathbf{x}\in\mathcal{X}, \mathbf{z}\in\mathcal{Z}} \{f(\mathbf{x}) + g(\mathbf{z}) :\ \mathbf{F}\mathbf{x} + \mathbf{G}\mathbf{z} = \mathbf{b}\} \tag{17}$$

where $f(\mathbf{x})$ and $g(\mathbf{z})$ are convex functions; $\mathcal{X}$ and $\mathcal{Z}$ are convex sets; and $(\mathbf{F}, \mathbf{G}, \mathbf{b})$ model the linear equality constraints coupling variables $\mathbf{x}$ and $\mathbf{z}$. In its normalized form, ADMM assigns a Lagrange multiplier $\mathbf{w}$ for the equality constraint and solves

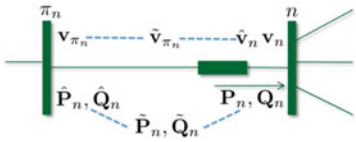

Fig. 2. Consensus and duplicate variables in the ADMM scheme. Variables connected by blue dotted lines are constrained to be equal.

(17) by iterating over the following three recursions

$$\mathbf{x}^{i+1} \in \arg\min_{\mathbf{x}\in\mathcal{X}} f(\mathbf{x}) + \tfrac{\rho}{2}\|\mathbf{F}\mathbf{x} + \mathbf{G}\mathbf{z}^i - \mathbf{b} + \mathbf{w}^i\|_2^2 \quad (18a)$$

$$\mathbf{z}^{i+1} \in \arg\min_{\mathbf{z}\in\mathcal{Z}} g(\mathbf{z}) + \tfrac{\rho}{2}\|\mathbf{F}\mathbf{x}^{i+1} + \mathbf{G}\mathbf{z} - \mathbf{b} + \mathbf{w}^i\|_2^2 \quad (18b)$$

$$\mathbf{w}^{i+1} := \mathbf{w}^i + \mathbf{F}\mathbf{x}^{i+1} + \mathbf{G}\mathbf{z}^{i+1} - \mathbf{b} \quad (18c)$$

for some $\rho > 0$. At iteration i, the primal and dual residual for (18) capturing primal and dual feasibility are defined as

$$o_p^i := \|\mathbf{F}\mathbf{x}^i + \mathbf{G}\mathbf{z}^i - \mathbf{b}\|_2$$
$$o_d^i := \rho\|\mathbf{F}^\top\mathbf{G}(\mathbf{z}^i - \mathbf{z}^{i-1})\|_2. \quad (19)$$

Under mild conditions, it has been shown that (o_p^i, o_d^i) converge to zero as the iteration index i goes to infinity, and that the objective function converges to the optimal value [26]. ADMM has been applied to decentralize various power system tasks [24], [27], [28]. Related ideas are adopted here to decouple the spatially-coupled constraints (16b)–(16d).

To that end, each bus $n \in \mathcal{N}$ maintains a local copy of the variables associated with the squared voltage magnitude of its parent bus, and the power flows feeding its children buses. These auxiliary variables are marked with a hat as $\hat{\mathbf{v}}_n$ and $\{(\hat{\mathbf{P}}_k, \hat{\mathbf{Q}}_k)\}_{k\in\mathcal{C}_n}$. The duplicate variable $\hat{\mathbf{v}}_n$ stored at bus n should agree with the original variable $\mathbf{v}_{\pi_n}$ stored at bus π_n as demonstrated in Fig. 2. To decentralize the computations, we further introduce the *consensus* variable $\tilde{\mathbf{v}}_{\pi_n}$, and impose the constraints $\mathbf{v}_{\pi_n} = \tilde{\mathbf{v}}_{\pi_n}$ and $\hat{\mathbf{v}}_n = \tilde{\mathbf{v}}_{\pi_n}$ for all non-leaf buses. The spatially-coupled equality constraints $\mathbf{v}_{\pi_n} = \tilde{\mathbf{v}}_{\pi_n}$ and $\hat{\mathbf{v}}_n = \tilde{\mathbf{v}}_{\pi_n}$ are dualized in the ADMM scheme. Consensus variables marked with a tilde are updated in the second step of ADMM, and all the remaining variables are updated in the first step of ADMM. By repeating this process for the power flow variables and for all $n \in \mathcal{N}$, the physical grid model is decoupled across buses.

We also introduce duplicate variables $\{\tilde{\mathbf{p}}_n^d(t)\}_{n\in\mathcal{N}}$ for net loads to separate the tasks of EV charging and generation dispatch. As detailed later, imposing the constraints $\tilde{\mathbf{p}}_n^d(t) = \mathbf{p}_n^d(t)$ for all n, enables isolating (16j) from the rest of the constraints in (16); resulting in localized EV charging subproblems that is a special case of (2).

For a compact representation define the aggregate variables:

$$\mathbf{x}_n(t) := \left\{\mathbf{v}_n(t), \mathbf{p}_n^g(t), \mathbf{p}_n^d(t), \mathbf{q}_n^g(t), \mathbf{P}_n(t), \mathbf{Q}_n(t)\right\}$$
$$\hat{\mathbf{x}}_n(t) := \left\{\hat{\mathbf{v}}_n(t), \{\hat{\mathbf{P}}_k(t), \hat{\mathbf{Q}}_k(t)\}_{k\in\mathcal{C}_n}\right\}$$
$$\tilde{\mathbf{z}}_n(t) := \left\{\tilde{\mathbf{v}}_n(t), \tilde{\mathbf{p}}_n^g(t), \tilde{\mathbf{p}}_n^d(t), \tilde{\mathbf{q}}_n^g(t), \tilde{\mathbf{P}}_n(t), \tilde{\mathbf{Q}}_n(t)\right\}$$

TABLE I
LAGRANGE MULTIPLIERS FOR PROBLEM (20)

$\mathbf{p}_n^g(t) = \tilde{\mathbf{p}}_n^g(t)$	$\boldsymbol{\lambda}_n^p(t)$	$\mathbf{q}_n^g(t) = \tilde{\mathbf{q}}_n^g(t)$	$\boldsymbol{\lambda}_n^q(t)$
$\tilde{\mathbf{P}}_n(t) = \hat{\mathbf{P}}_n(t)$	$\hat{\boldsymbol{\lambda}}_n^P(t)$	$\mathbf{P}_n(t) = \tilde{\mathbf{P}}_n(t)$	$\boldsymbol{\lambda}_n^P(t)$
$\tilde{\mathbf{Q}}_n(t) = \hat{\mathbf{Q}}_n(t)$	$\hat{\boldsymbol{\lambda}}_n^Q(t)$	$\mathbf{Q}_n(t) = \tilde{\mathbf{Q}}_n(t)$	$\boldsymbol{\lambda}_n^Q(t)$
$\hat{\mathbf{v}}_n(t) = \tilde{\mathbf{v}}_{\pi_n}(t)$	$\hat{\boldsymbol{\lambda}}_n^v(t)$	$\mathbf{v}_n(t) = \tilde{\mathbf{v}}_n(t)$	$\boldsymbol{\lambda}_n^v(t)$
$\mathbf{p}_n^d(t) = \tilde{\mathbf{p}}_n^d(t)$	$\boldsymbol{\lambda}_n^d(t)$	Constraints (20l)	$\mu_{n,\phi}(t)$

for all $n \in \mathcal{N}$ and $t \in \mathcal{T}$. With the newly introduced variables, problem (16) can be equivalently expressed as:

$$\min \sum_{t\in\mathcal{T}}\left[f_0(\mathbf{P}_0(t)) + \sum_{n\in\mathcal{N}} f_n^g(\tilde{\mathbf{p}}_n^g(t))\right] \quad (20a)$$

$$\text{over } \{\mathbf{x}_n(t), \hat{\mathbf{x}}_n(t), \tilde{\mathbf{z}}_n(t)\}_{n\in\mathcal{N},t\in\mathcal{T}},\ \{\mathbf{e}_m \in \mathcal{E}_m\}_{m\in\mathcal{M}},$$

$$\text{s.to } \mathbf{p}_n^g(t) - \mathbf{p}_n^d(t) = \sum_{k\in\mathcal{C}_n}\hat{\mathbf{P}}_k(t) - \mathbf{P}_n(t), \forall\, n \in \mathcal{N}, t \quad (20b)$$

$$\mathbf{q}_n^g(t) - \mathbf{q}_n^d(t) = \sum_{k\in\mathcal{C}_n}\hat{\mathbf{Q}}_k(t) - \mathbf{Q}_n(t), \forall\, n \in \mathcal{N}, t \quad (20c)$$

$$\hat{\mathbf{v}}_n(t) - \mathbf{v}_n(t) = \mathrm{Re}\{\bar{\mathbf{Z}}_n(\mathbf{P}_n(t) + j\mathbf{Q}_n(t))\} \quad \forall n \in \mathcal{N}^+, t \quad (20d)$$

$$\underline{p}_{n,\phi}^g \le \tilde{p}_{n,\phi}^g(t) \le \bar{p}_{n,\phi}^g,\ \forall\,\phi \in \mathcal{P}_n, n \in \mathcal{N}, t \quad (20e)$$

$$\underline{q}_{n,\phi}^g \le \tilde{q}_{n,\phi}^g(t) \le \bar{q}_{n,\phi}^g,\ \forall\,\phi \in \mathcal{P}_n, n \in \mathcal{N}, t \quad (20f)$$

$$\underline{v}_n \le \tilde{v}_{n,\phi}(t) \le \bar{v}_n,\ \forall\,\phi \in \mathcal{P}_n, n \in \mathcal{N}, t \quad (20g)$$

$$\tilde{P}_{n,\phi}^2(t) + \tilde{Q}_{n,\phi}^2(t) \le \bar{S}_n^2,\ \forall\,\phi \in \mathcal{P}_n, n \in \mathcal{N}_+, t \quad (20h)$$

$$\mathbf{P}_n(t) = \tilde{\mathbf{P}}_n(t),\ \mathbf{Q}_n(t) = \tilde{\mathbf{Q}}_n(t),\ \mathbf{v}_n(t) = \tilde{\mathbf{v}}_n(t), \quad \forall\, n \in \mathcal{N}^+, t \quad (20i)$$

$$\hat{\mathbf{P}}_n(t) = \tilde{\mathbf{P}}_n(t),\ \hat{\mathbf{Q}}_n(t) = \tilde{\mathbf{Q}}_n(t),\ \hat{\mathbf{v}}_n(t) = \tilde{\mathbf{v}}_{\pi_n}(t), \quad \forall\, n \in \mathcal{N}^+, t \quad (20j)$$

$$\mathbf{p}_n^g(t) = \tilde{\mathbf{p}}_n^g(t), \mathbf{p}_n^d(t) = \tilde{\mathbf{p}}_n^d(t), \mathbf{q}_n^g(t) = \tilde{\mathbf{q}}_n^g(t), \quad \forall\, n \in \mathcal{N}, t \quad (20k)$$

$$\tilde{p}_{n,\phi}^d(t) = d_{n,\phi}(t) + \sum_{m\in\mathcal{M}_{n,\phi}} e_m(t),\ \forall\phi \in \mathcal{P}_n, n, t \quad (20l)$$

$$(\mathbf{1}^\top\tilde{\mathbf{P}}_0(t))^2 + (\mathbf{1}^\top\tilde{\mathbf{Q}}_0(t))^2 \le \bar{S}_f^2,\ \forall t. \quad (20m)$$

The equality constraints between duplicate variables in (20i)–(20l) are assigned Langrange multipliers according to Table I. Adopting the ADMM iterates of (18) to solve (20), variables $\{\mathbf{x}_n(t), \hat{\mathbf{x}}_n(t)\}_{n\in\mathcal{N},t\in\mathcal{T}}$ and $\{\mathbf{e}_m\}_{m\in\mathcal{M}}$ are updated in the first

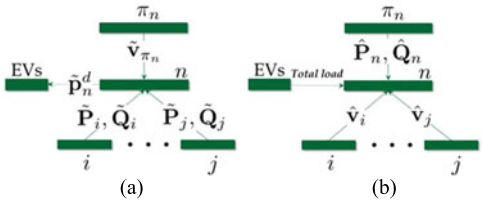

Fig. 3. Information exchange in the ADMM steps for bus n. (a) First step of ADMM. (b) Second step of ADMM.

ADMM step, whereas variables $\{\{\tilde{\mathbf{z}}_n(t)\}_{n\in\mathcal{N}}\}_{t\in\mathcal{T}}$ are updated during the second ADMM step as detailed next.

A. First Step of ADMM

Due to the form the generic update (18a) takes for the problem at hand, variables $\{\mathbf{x}_n(t), \hat{\mathbf{x}}_n(t)\}_{n\in\mathcal{N},t\in\mathcal{T}}$ can be updated separately from the EV charging profiles $\{\mathbf{e}_m\}_{m\in\mathcal{M}}$. The updates for these two variable sets are studied next.

Heed that $\{\mathbf{x}_n(t), \hat{\mathbf{x}}_n(t)\}_{n\in\mathcal{N},t\in\mathcal{T}}$ can be optimized independently across buses and time periods. Nevertheless, for fixed bus and time indices (n,t), variables $\mathbf{x}_n(t)$ and $\hat{\mathbf{x}}_n(t)$ are coupled due to constraints (20b)–(20d). To simplify the presentation, we drop the time index and consider the canonical subproblems involved for all $t\in\mathcal{T}$. Let $\hat{\mathbf{z}}_n := \left\{\tilde{\mathbf{v}}_{\pi_n}, \{\tilde{\mathbf{P}}_k, \tilde{\mathbf{Q}}_k\}_{k\in\mathcal{C}_n}\right\}$ for bus $n\in\mathcal{N}^+$. Variables $\mathbf{x}_n$ and $\hat{\mathbf{x}}_n$ are updated during the ith iteration as the minimizers of

$$\min_{\mathbf{x}_n,\hat{\mathbf{x}}_n} \ \|\mathbf{x}_n - \mathbf{z}_n^i + \boldsymbol{\lambda}_n^i\|_2^2 + \|\hat{\mathbf{x}}_n - \hat{\mathbf{z}}_n^i + \hat{\boldsymbol{\lambda}}_n^i\|_2^2$$
$$\text{s.to } (20b)-(20d). \tag{21}$$

For $n=0$ and due to the power supply cost from the main grid, variables $(\mathbf{P}_0, \mathbf{Q}_0)$ are found as the minimizers of

$$\min_{\mathbf{P}_0,\mathbf{Q}_0} \ \|\mathbf{x}_0 - \mathbf{z}_0^i + \boldsymbol{\lambda}_0^i\|_2^2 + \|\hat{\mathbf{x}}_0 - \hat{\mathbf{z}}_0^i + \hat{\boldsymbol{\lambda}}_0^i\|_2^2 + \frac{2}{\rho} f_0(\mathbf{P}_0)$$
$$\text{s.to } (20b)-(20c). \tag{22}$$

Problems (21), (22) are linearly-constrained quadratic programs with closed-form minimizers [20].

We next focus on updating the vehicle charging profiles $\{\mathbf{e}_m\}_{m\in\mathcal{M}}$ at iteration i. Interestingly, the task of EV charging decouples over buses and phases. The charging profiles for vehicles $m\in\mathcal{M}_{n,\phi}$ can be updated as the minimizers of

$$\min_{\{\mathbf{e}_m\in\mathcal{E}_m\}_{m\in\mathcal{M}_{n,\phi}}} \frac{1}{2}\sum_{t\in\mathcal{T}}\left(l_{n,\phi}^i(t) + \sum_{m\in\mathcal{M}_{n,\phi}} e_m(t)\right)^2 \tag{23}$$

where $l_{n,\phi}^i(t) := d_{n,\phi}(t) - \tilde{p}_{n,\phi}^{d,i}(t) + \mu_{n,\phi}^i(t)$ and the Lagrange multiplier $\mu_{n,\phi}^i(t)$ reflects the network constraints. Note (23) is actually a special case of (2) with $C_t(x) = x^2/2$, $\forall t$. Hence, subproblem (23) can be solved using Alg. 1.

In the first step of ADMM, each bus n needs to collect $\tilde{\mathbf{v}}_{\pi_n}$ from its parent and $\{\tilde{\mathbf{P}}_k, \tilde{\mathbf{Q}}_k\}_{k\in\mathcal{C}_n}$ from all its children as depicted in Fig. 3(a). Meanwhile, each bus n transfers $\tilde{\mathbf{p}}_n^d$ to its EV scheduling center, where the charging profile of EVs are optimized using Alg. 1.

B. Second Step of ADMM

Finding optimal $\{\tilde{\mathbf{z}}_n(t)\}_{n\in\mathcal{N},t\in\mathcal{T}}$ can be performed independently across buses and time slots. Because of that, time indices are ignored. Every bus n has to solve five sub-problems in parallel, each one associated with the variables $\tilde{\mathbf{p}}_n^g$, $\tilde{\mathbf{p}}_n^d$, $\tilde{\mathbf{q}}_n^g$, $\tilde{\mathbf{v}}_n$, and $(\tilde{\mathbf{P}}_n, \tilde{\mathbf{Q}}_n)$. Firstly, updating $\tilde{\mathbf{p}}_n^g$, $\tilde{\mathbf{p}}_n^d$, $\tilde{\mathbf{q}}_n^g$, and $\tilde{\mathbf{v}}_n$ decouples over phases of bus n too. It can be shown that per phase variables are updated as the minimizers of a univariate convex quadratic function possibly over box constraints. If the generation cost at bus n is $f_n^g(\tilde{\mathbf{p}}_n^g) := \sum_{\phi\in\mathcal{P}_n} a_{n,\phi}(p_{n,\phi}^g)^2 + b_{n,\phi}p_{n,\phi}^g + c_{n,\phi}$ with $a_{n,\phi}\geq 0$, then $\tilde{p}_{n,\phi}^g$ is updated at iteration i by solving

$$\min_{\tilde{p}_{n,\phi}^g} \ a_{n,\phi}(\tilde{p}_{n,\phi}^g)^2 + b_{n,\phi}\tilde{p}_{n,\phi}^g + \tfrac{\rho}{2}(p_{n,\phi}^{g,i} - \tilde{p}_{n,\phi}^g + \lambda_{n,\phi}^{p,i})^2$$
$$\text{s.to } \underline{p}_{n,\phi}^g \leq \tilde{p}_{n,\phi}^g \leq \bar{p}_{n,\phi}^g. \tag{24}$$

The minimizer of (24) is expressed as

$$\tilde{p}_{n,\phi}^{g,i+1} = \left[\frac{\rho(p_{n,\phi}^{g,i} + \lambda_{n,\phi}^{p,i}) - b_{n,\phi}}{2a_{n,\phi}+\rho}\right]_{\underline{p}_{n,\phi}^g}^{\bar{p}_{n,\phi}^g} \tag{25}$$

where $[x]_{\underline{x}}^{\bar{x}} := \max\{\underline{x}, \min\{x,\bar{x}\}\}$. The entries of $\tilde{\mathbf{q}}_n^g$ and $\tilde{\mathbf{v}}_n$ are similarly found as

$$\tilde{q}_{n,\phi}^{g,i+1} = \left[q_{n,\phi}^{g,i} + \lambda_{n,\phi}^{q,i}\right]_{\underline{q}_{n,\phi}^g}^{\bar{q}_{n,\phi}^g} \tag{26}$$

$$\tilde{v}_{n,\phi}^{i+1} = \left[\frac{\sum_{k\in\mathcal{C}_n}(\hat{v}_{k,\phi}^i + \hat{\lambda}_{k,\phi}^{v,i}) + v_{n,\phi}^i + \lambda_{n,\phi}^{v,i}}{|\mathcal{C}_n|+1}\right]_{\underline{v}_n}^{\bar{v}_n}. \tag{27}$$

The entries of $\tilde{\mathbf{p}}_n^d$ are obtained as the solutions of unconstrained univariate convex quadratic programs as

$$\tilde{p}_{n,\phi}^{d,i+1} = \frac{1}{2}\left(p_{n,\phi}^{d,i} + \lambda_{n,\phi}^{d,i} + d_{n,\phi} + \sum_{m\in\mathcal{M}_{n,\phi}} e_m^i + \mu_{n,\phi}^i\right). \tag{28}$$

The optimizations involved in updating the consensus power flow variables $\{\tilde{\mathbf{P}}_n, \tilde{\mathbf{Q}}_n\}_{n\in\mathcal{N}^+}$ decouple across phases. The consensus power flow variables $\{(\tilde{P}_{n,\phi}, \tilde{Q}_{n,\phi})\}_{\phi\in\mathcal{P}_n, n\in\mathcal{N}^+}$ are updated by solving the problems for all $\phi\in\mathcal{P}_n$ and $n\in\mathcal{N}^+$:

$$\min_{\tilde{P}_{n,\phi},\tilde{Q}_{n,\phi}} \ (\tilde{P}_{n,\phi} - \breve{P}_{n,\phi}^i)^2 + (\tilde{Q}_{n,\phi} - \breve{Q}_{n,\phi}^i)^2 \tag{29}$$
$$\text{s.to } \tilde{P}_{n,\phi}^2 + \tilde{Q}_{n,\phi}^2 \leq \bar{S}_n^2$$

where $\breve{P}_{n,\phi}^i := \frac{1}{2}(P_{n,\phi}^i + \hat{P}_{n,\phi}^i + \lambda_{n,\phi}^{P,i} + \hat{\lambda}_{n,\phi}^{P,i})$, and $\breve{Q}_{n,\phi}^i := \frac{1}{2}(Q_{n,\phi}^i + \hat{Q}_{n,\phi}^i + \lambda_{n,\phi}^{Q,i} + \hat{\lambda}_{n,\phi}^{Q,i})$. Resorting to the KKT

Algorithm 3: Decentralized *network-constrained* charging.

1: Initialize $\mathbf{e}_m^0 = \mathbf{0}$ for all m.
2: **for** $i = 0, 1, \ldots$ **do** (parallel across all buses)
3: Bus n solves (21) or (22) to obtain $\mathbf{x}_n^{i+1}$ and $\hat{\mathbf{x}}_n^{i+1}$.
4: Bus n solves (23) via Alg. 1 to update $\mathbf{e}_m^{i+1}$ for $m \in \mathcal{M}_n$.
5: Bus n updates $\tilde{\mathbf{z}}_n^{i+1}$ from (24)–(28), (30), and (32).
6: Bus n updates Lagrange multipliers by (18c).
7: **end for**

conditions for (29) shows that its minimizers are

$$\tilde{P}_{n,\phi}^{i+1} := \min\left\{\frac{\bar{S}_n}{\sqrt{(\breve{P}_{n,\phi}^i)^2 + (\breve{Q}_{n,\phi}^i)^2}}, 1\right\} \breve{P}_{n,\phi}^i \tag{30a}$$

$$\tilde{Q}_{n,\phi}^{i+1} := \min\left\{\frac{\bar{S}_n}{\sqrt{(\breve{P}_{n,\phi}^i)^2 + (\breve{Q}_{n,\phi}^i)^2}}, 1\right\} \breve{Q}_{n,\phi}^i. \tag{30b}$$

The substation power flows are updated as the solution to

$$\min_{\tilde{\mathbf{P}}_0, \tilde{\mathbf{Q}}_0} \ \|\tilde{\mathbf{P}}_0 - \breve{\mathbf{P}}_0^i\|_2^2 + \|\tilde{\mathbf{Q}}_0 - \breve{\mathbf{Q}}_0^i\|_2^2 \tag{31}$$
$$\text{s.to } (\mathbf{1}^\top \tilde{\mathbf{P}}_0)^2 + (\mathbf{1}^\top \tilde{\mathbf{Q}}_0)^2 \leq \bar{S}_f^2$$

where $\breve{\mathbf{P}}_0^i := \mathbf{P}_0^i + \boldsymbol{\lambda}_0^{P,i}$ and $\breve{\mathbf{Q}}_0^i := \mathbf{Q}_0^i + \boldsymbol{\lambda}_0^{Q,i}$. The minimizers of (31) can be computed in closed-form as shown in the Appendix:

Proposition 1: The optimal solution of problem (31) is

$$\tilde{\mathbf{P}}_0^{i+1} := \breve{\mathbf{P}}_0^i - \max\left\{1 - \frac{\bar{S}_f}{\Sigma}, 0\right\} \frac{\mathbf{1}\mathbf{1}^\top \breve{\mathbf{P}}_0^i}{3} \tag{32a}$$

$$\tilde{\mathbf{Q}}_0^{i+1} := \breve{\mathbf{Q}}_0^i - \max\left\{1 - \frac{\bar{S}_f}{\Sigma}, 0\right\} \frac{\mathbf{1}\mathbf{1}^\top \breve{\mathbf{Q}}_0^i}{3} \tag{32b}$$

where $\Sigma := \sqrt{(\mathbf{1}^\top \breve{\mathbf{P}}_0^i)^2 + (\mathbf{1}^\top \breve{\mathbf{Q}}_0^i)^2}$.

To implement the second step of ADMM, bus n gathers its copies $(\hat{\mathbf{P}}_n, \hat{\mathbf{Q}}_n)$ from its parent, $\{\hat{v}_k\}_{k \in \mathcal{C}_n}$ from all its children, and the total charging load $\{\sum_{m \in \mathcal{M}_{n,\phi}} \mathbf{e}_m^k\}_{\phi \in \mathcal{P}_n}$ of all the connected EVs as presented in Fig. 3(b). Then bus n updates $\tilde{\mathbf{z}}_n$ according to (24)–(28), (30), and (32).

C. Third Step of ADMM

The Lagrange multipliers are updated according to (18c), i.e., every multiplier is equal to its previous value plus the most recent constraint violation. The overall information exchange for the devised algorithm is depicted in Fig. 3, while the charging protocol is summarized as Algorithm 3.

V. Numerical Tests

A. Frank–Wolfe Scheme for Vehicle Charging

We first evaluated Alg. 1 by simulating the charging of 59 EVs. The costs are selected as $C_t(x) := x^2/2$ for all t [10]. For all vehicles, the battery capacity was 20 kWh and the maximum charging rate was 3.45 kW [15]. The plug-in/-out times and daily travel miles were set according to statistical estimates obtained from the National Household Travel Survey [29], [30].

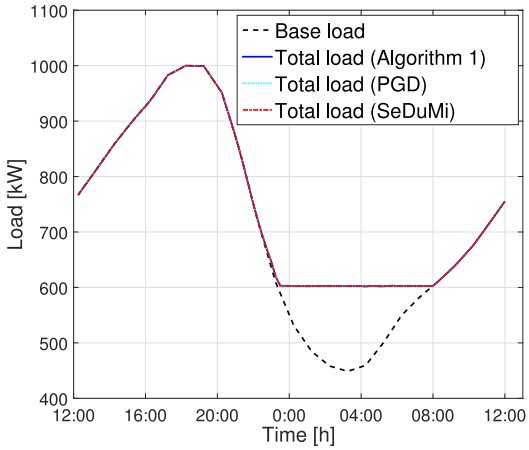

Fig. 4. Load curves after optimal charging of 59 EVs.

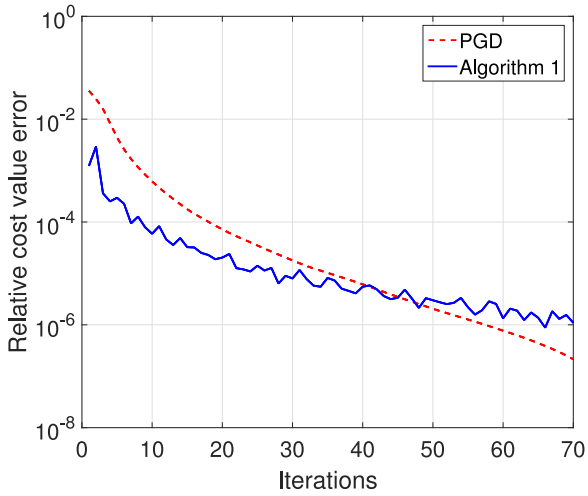

Fig. 5. Cost convergence for Alg. 1 and PGD.

The expected state of charge for EVs was fixed to 90%, and the energy needed per 100 km is $E_{100} = 15$ kWh. The initial state of charge for EV m was modeled as $s_m^{soc} = 0.9 - D_m^{\text{miles}} E_{100}/(100 B_m)$ for daily travel miles D_m^{miles}. The normalized base load curves were obtained by averaging the 2014 residential load data from Southern California Edison. A day-long horizon starting at midnight was divided into $T = 96$ slots. Tests were run on MATLAB using an Intel CPU @ 3.6 GHz (32 GB RAM) computer.

Parameter $d(t)$ was the normalized residential load with the maximum load set to 1000 kW [10]. The minimizer of (16) was obtained via SeDuMi, Algorithm 1, and the PGD solver of [10]. The subproblem (13) in PGD was solved by SeDuMi. Algorithm 1 and PGD were run sequentially and they were terminated once the relative cost error became smaller than 10^{-6}. Fig. 4 shows that the three resultant load curves coincide and

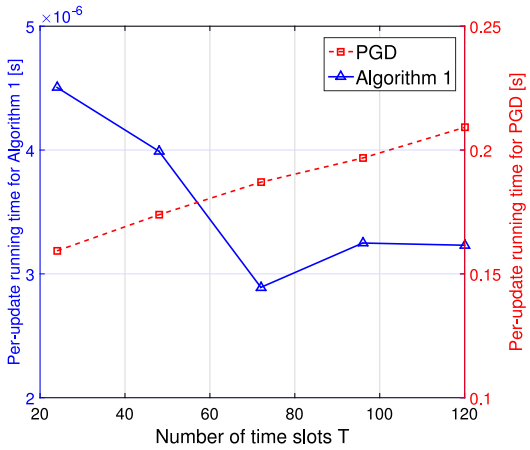

Fig. 6. Average update time for Alg. 1 and PGD.

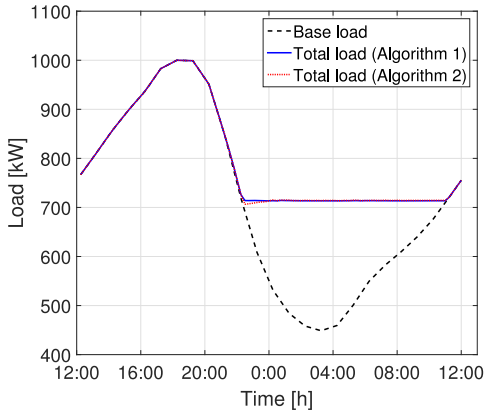

Fig. 7. Load curves after optimal charging of 120 EVs. The performance degradation using the online Alg. 7 is very small.

feature a flat load valley. Algorithm 1 converged within 0.01 sec, PGD in 12.5 sec, and SeDuMi in 82.47 sec. Problem (2) was also solved by the ADMM-based scheme of [8] that converged in 13 sec. Similar to PGD, each ADMM update of the latter involves a quadratic program per vehicle.

Fig. 5 depicts the cost convergence curves for Alg. 1 and PGD while scheduling 59 vehicles over $T = 96$ time slots. Fig. 6 presents the mean running times (averaged across vehicles and iterations) of a single update of Alg. 1 and PGD and for varying T. Although Alg. 1 attains a relative cost function error of 10^{-6} at roughly the same rate as PGD, its mean update time is in the order of microseconds, whereas PGD's mean time is in the order of seconds and increases linearly with T. The major computational advantage of Alg. 1 is the simple update in (10).

The real-time Alg. 2 was subsequently evaluated. By simulating the same 59 EVs used in our first experiment, Alg. 2 exhibited a load curve almost identical to the one obtained by the offline Alg. 1 in Fig. 4. To amplify the effects of random charging requests, the number of simulated EVs was increased to 120. According to the total load curves shown in Fig. 7, the two charging protocols differ slightly around 23:00, thus verifying the efficiency of Alg. 2. Similar observations have also been made in [10] for uniformly distributed plug-in times. Compared to the PGD protocol of [10], the computational advantage of Alg. 2 enables faster real-time EV scheduling.

B. ADMM-Based Scheme for Network-Constrained Charging

Algorithm 3 was first tested using the unbalanced IEEE 13-bus feeder [31]. Voltage magnitudes were constrained within $[\underline{v}, \bar{v}] = [0.97, 1.03]$ pu and the feeder voltage was set to 1 pu. The cost of energy drawn from the main grid was $f_0(\mathbf{P}_0) := \sum_\phi f_{0,\phi}(P_{0,\phi})$, where $f_{0,\phi}(P_{0,\phi}) := a_{0,\phi} P_{0,\phi}^2 + b_{0,\phi} P_{0,\phi}$, $a_{0,\phi} = 0.1\$/(\text{MW})^2\text{h}$, and $b_{0,\phi} = 16\,\$/\text{MWh}$ for all three phases ϕ. Two distributed generators (DG) were located at buses 2 and 13. Their generation costs had the same functional form as $f_0(\mathbf{P}_0)$ with coefficients $a_{n,\phi} = 0.1\,\$/(\text{MW})^2\text{h}$, and $b_{n,\phi} = 8\,\$/\text{MWh}$ for all three phases ϕ and $n = 2, 13$. Forty eight EVs were being charged on phases b and c of bus 6 and phase a of bus 13 (16 EVs per location) resulting in a total of 23 328 variables for $T = 96$ time slots. SeDuMi and Alg. 3 converged to the optimal cost of \$744.76 within 454 sec and 4.76 sec, respectively. The convergence of the objective in (16) shown in Fig. 8(a) and the evolution of $o_p^i/T\sqrt{N}$ and $o_d^i/T\sqrt{N}$ shown in Fig. 8(b) demonstrate that Alg. 3 converged within 350 iterations. Elaborating on the running time, the average running time for solving the vehicle scheduling subproblem (23) using Alg. 1 was $8.6 \cdot 10^{-3}$ sec, and the average time spent on the remaining ADMM updates was $5 \cdot 10^{-3}$ sec. The overall computational efficiency of Alg. 3 is due to the closed-form updates and the use of Alg. 1 to tackle (23).

To evaluate the scalability of Alg. 3, vehicle numbers were increased to 24 on phase b of bus 6, 24 on phase c of bus 6, and 20 on phase a of bus 13. For this setup, SeDuMi and Alg. 3 reached the optimal cost of \$748.98 in 713 sec and 4.80 sec, respectively. The average running time for tackling (23) using Alg. 1 took $8.7 \cdot 10^{-3}$ sec, and the average time spent on the remaining ADMM updates was $5 \cdot 10^{-3}$ sec as before. For a total of 350 iterations, the total running time for Alg. 3 was 4.8 sec, slightly larger than the previous case.

Due to the flexibility of EV loads to be served at night, no voltage constraint was active during the previous experiments. To test the effect of network constraints, the DG cost at bus 13 was increased by setting $a_{13,\phi} = 2\$/(\text{MW})^2\text{h}$, and $b_{13,\phi} = 16\,\$/\text{MWh}$ for all three phases ϕ. Moreover, the capacitor at the same bus was removed. The result was additional active power flowing from the feeder bus with less reactive power support thus causing undervoltage scenarios. Sixteen vehicles were assumed on phases b and c of bus 6 and phase a of bus 13. SeDuMi and Alg. 3 converged to the optimal cost of \$881.44 in 562 sec and 12 sec (700 iterations), respectively. The voltage magnitude on phase c of bus 13 was reaching the lower limit of 0.97 pu from time slot 6 to 38. Without considering network constraints, the voltage magnitude on phase c of bus 13 would drop to 0.96 pu, and the total cost would decrease to \$861.15.

Algorithm 3 was also tested on the larger unbalanced IEEE 123-bus feeder [31]. Fifteen DG units were placed in the system; while 5, 10, 15, 25 and 5 vehicles were being charged on buses 3, 15, 64, 82, and 102, respectively. In this feeder scenario, SeDuMi was unable to handle the 182,880 variables involved

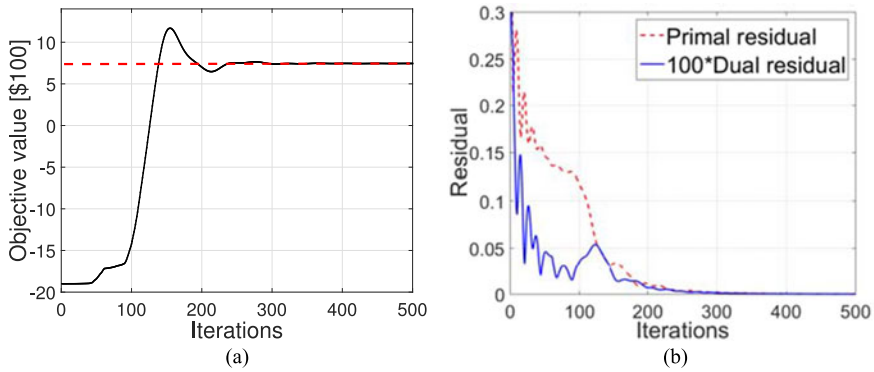

Fig. 8. Convergence performance for the IEEE 13-bus feeder. (a) Convergence of objective value. (b) Primal/dual residual convergence.

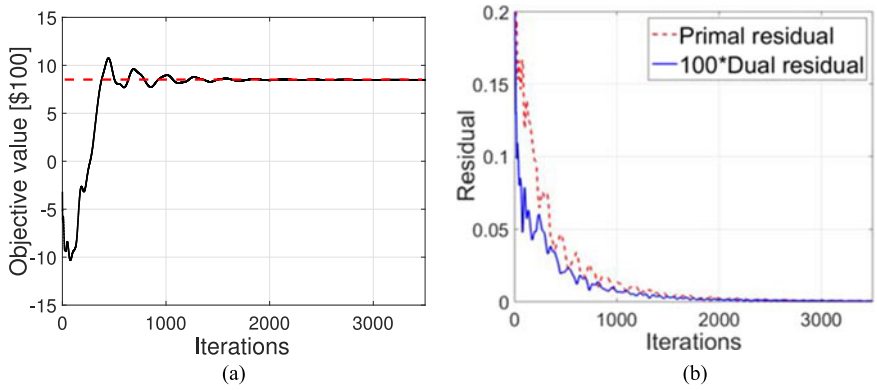

Fig. 9. Convergence performance for the IEEE 123-bus feeder. (a) Objective value convergence. (b) Primal/dual residual convergence.

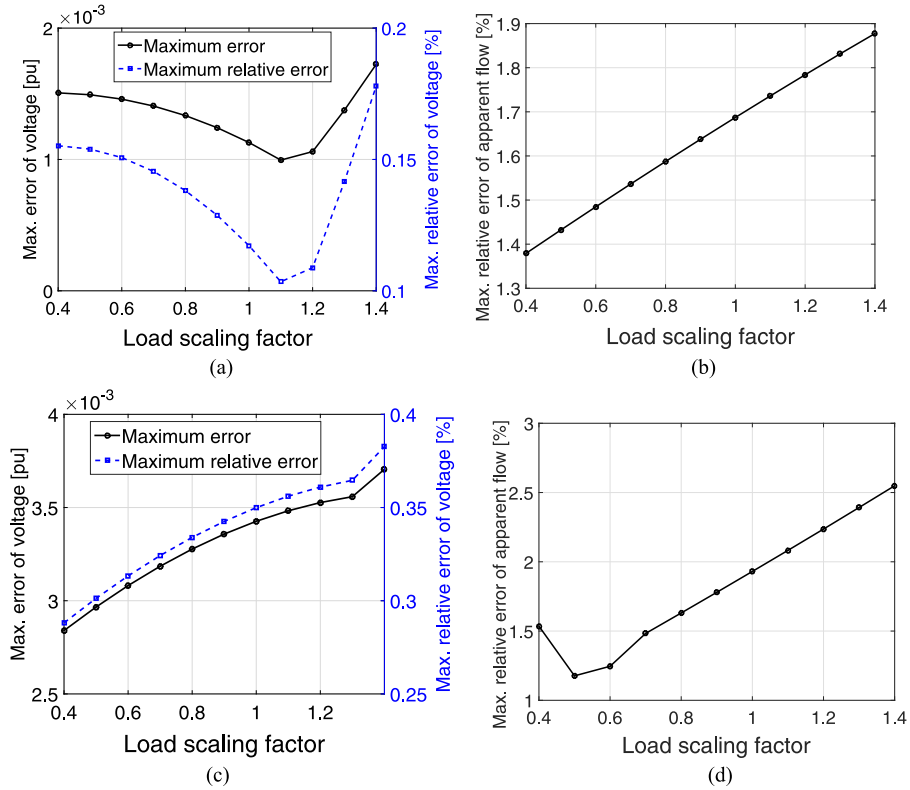

Fig. 10. Approximation error between the full ac and the linearized power flow models for increasing loading factor. (a) Voltages in 13-bus feeder. (b) Apparent flows in 13-bus feeder. (c) Voltages in 123-bus feeder. (d) Apparent flows in 123-bus feeder.

over $T = 96$ slots. The cost convergence and the convergence of $o_p^i/T\sqrt{N}$ and $o_d^i/T\sqrt{N}$ are shown in Fig. 9. The optimum cost of \$849.43 was attained in 2,000 iterations. The average running times for (23) and for the remaining ADMM subproblems were $8.4 \cdot 10^{-3}$ sec and $4.7 \cdot 10^{-3}$ sec, respectively, resulting in 26 sec for Alg. 3 to converge.

Finally, the approximation error incurred by the linearized grid model in (15c) was also examined. The full ac power flow model was solved using the forward-backward sweep algorithm [32]. The approximation error was numerically evaluated by varying active loads from 0.4 to 1.4 times the original peak load while maintaining the power factor constant. The maximum error and the maximum relative error in voltage magnitudes over all phases and buses are shown in Fig. 10(a) and (c), respectively for the IEEE 13-bus and the 123-bus feeders. The voltage approximation error is less than $4 \cdot 10^{-3}$ pu. Fig. 10(b) and (d) depict the maximum relative errors in apparent power flows, which are within 3%.

VI. Conclusion

Given that optimal EV charging scales unfavorably with the fleet size and the number of control periods, decentralized charging protocols have been developed in this work. A simple vehicle charging scheme has been devised based on Frank–Wolfe iterations. This charging protocol exhibits provable $\mathcal{O}(\frac{1}{k})$ convergence, poses minimal computational requirements to EV controllers, enjoys privacy and security features, and attains a 100-times acceleration in terms of computational time over existing alternatives. To accommodate scenarios where EVs plug-in sequentially, a real-time scheduling scheme has also been developed. To respect voltage and feeder transformer limits, network-constrained EV charging has been considered too. To achieve scalability, an ADMM-based solver has been built leveraging an approximate grid model. The solver features closed-form updates and incorporates the scheduling protocol of vehicle charging. Numerical tests using real-world data verify the optimality and efficiency of the proposed decentralized schemes. Extensions to asynchronous ADMM and Frank–Wolfe updates constitute current research directions.

Appendix

Proof of Prop. 1 The Lagrangian function of the convex problem in (31) reads $L(\tilde{\mathbf{P}}_0, \tilde{\mathbf{Q}}_0, \nu) = \|\tilde{\mathbf{P}}_0 - \breve{\mathbf{P}}_0^i\|_2^2 + \|\tilde{\mathbf{Q}}_0 - \breve{\mathbf{Q}}_0^i\|_2^2 + \nu\left[(\mathbf{1}^\top\tilde{\mathbf{P}}_0)^2 + (\mathbf{1}^\top\tilde{\mathbf{Q}}_0)^2 - \bar{S}_f^2\right]$. Because (31) satisfies Slater's condition (e.g., for $\tilde{\mathbf{P}}_0 = \tilde{\mathbf{Q}}_0 = \mathbf{0}$), strong duality holds [20]. If $(\tilde{\mathbf{P}}_0^*, \tilde{\mathbf{Q}}_0^*, \nu^*)$ are the optimal primal/dual variables, Lagrangian optimality yields:

$$\tilde{\mathbf{P}}_0^* - \breve{\mathbf{P}}_0^i + \nu^* \mathbf{1}\mathbf{1}^\top\tilde{\mathbf{P}}_0^* = \mathbf{0} \tag{33a}$$

$$\tilde{\mathbf{Q}}_0^* - \breve{\mathbf{Q}}_0^i + \nu^* \mathbf{1}\mathbf{1}^\top\tilde{\mathbf{Q}}_0 = \mathbf{0}. \tag{33b}$$

Premultiplying both sides of (33a), (33b) by $\mathbf{1}^\top$ results in:

$$\mathbf{1}^\top\tilde{\mathbf{P}}_0^* = \frac{\mathbf{1}^\top\breve{\mathbf{P}}_0^i}{1+3\nu^*} \quad \text{and} \quad \mathbf{1}^\top\tilde{\mathbf{Q}}_0^* = \frac{\mathbf{1}^\top\breve{\mathbf{Q}}_0^i}{1+3\nu^*}. \tag{34}$$

Complementary slackness yields $\nu^*\left[(\mathbf{1}^\top\tilde{\mathbf{P}}_0^*)^2 + (\mathbf{1}^\top\tilde{\mathbf{Q}}_0^*)^2 - \bar{S}_f^2\right] = 0$, which from (34) and dual feasibility provides

$$\nu^* = 0 \text{ or } \nu^* = \frac{1}{3}\left(\sqrt{(\mathbf{1}^\top\breve{\mathbf{P}}_0^i)^2 + (\mathbf{1}^\top\breve{\mathbf{Q}}_0^i)^2}/\bar{S}_f - 1\right). \tag{35}$$

The claim follows from primal feasibility, (33), and (35). ■

References

[1] P. Richardson, D. Flynn, and A. Keane, "Optimal charging of electric vehicles in low-voltage distribution systems," *IEEE Trans. Power Syst.*, vol. 27, no. 1, pp. 268–279, Feb. 2012.

[2] Y. Cao *et al.*, "An optimized EV charging model considering TOU price and SOC curve," *IEEE Trans. Smart Grid*, vol. 3, no. 1, pp. 388–393, Mar. 2012.

[3] S. Shao, M. Pipattanasomporn, and S. Rahman, "Challenges of PHEV penetration to the residential distribution network," in *Proc. Power & Energy Soc. General Meeting*, Calgary, AB, Canada, Jul. 2009, pp. 1–6.

[4] Z. Fan, "A distributed demand response algorithm and its application to PHEV charging in smart grids," *IEEE Trans. Smart Grid*, vol. 3, no. 3, pp. 1280–1290, Sep. 2012.

[5] Z. Ma, D. Callaway, and I. Hiskens, "Decentralized charging control for large populations of plug-in electric vehicles," in *Proc. 49th IEEE Conf. Decision Control*, Atlanta, GA, USA, Dec. 2010, pp. 206–212.

[6] N. Gatsis and G. B. Giannakis, "Residential load control: Distributed scheduling and convergence with lost AMI messages," *IEEE Trans. Smart Grid*, vol. 3, no. 2, pp. 770–786, Jun. 2012.

[7] C. Shao, X. Wang, X. Wang, and C. Du, "Layered and distributed charge load dispatch of considerable electric vehicles," *IEEE Trans. Power Syst.*, vol. 30, no. 4, pp. 1858–1867, Jul. 2015.

[8] J. Rivera, P. Wolfrum, S. Hirche, C. Goebel, and H.-A. Jacobsen, "Alternating direction method of multipliers for decentralized electric vehicle charging control," in *Proc. Conf. Decision Control*, Florence, Italy, Dec. 2013, pp. 6960–6965.

[9] R. Li, Q. Wu, and S. Oren, "Distribution locational marginal pricing for optimal electric vehicle charging management," *IEEE Trans. Power Syst.*, vol. 29, no. 1, pp. 203–211, Jan. 2014.

[10] L. Gan, U. Topcu, and S. Low, "Optimal decentralized protocol for electric vehicle charging," *IEEE Trans. Power Syst.*, vol. 28, no. 2, pp. 940–951, May 2013.

[11] E. L. Karfopoulos and N. D. Hatziargyriou, "A multi-agent system for controlled charging of a large population of electric vehicles," *IEEE Trans. Power Syst.*, vol. 28, no. 2, pp. 1196–1204, May 2013.

[12] W.-J. Ma, V. Gupta, and U. Topcu, "On distributed charging control of electric vehicles with power network capacity constraints," in *Proc. Amer. Control Conf.*, Portland, OR, USA, Jun. 2014, pp. 4306–4311.

[13] O. Ardakanian, C. Rosenberg, and S. Keshav, "Distributed control of electric vehicle charging," in *Proc. Int. Conf. Future Energy Syst.*, Berkeley, CA, USA, May 2013, pp. 101–112.

[14] W.-J. Ma, V. Gupta, and U. Topcu, "Distributed charging control of electric vehicles using regret minimization," in *Proc. IEEE Conf. Decision Control*, Los Angeles, CA, USA, Dec. 2014, pp. 4917–4923.

[15] J. de Hoog, T. Alpcan, M. Brazil, D. Thomas, and I. Mareels, "Optimal charging of electric vehicles taking distribution network constraints into account," *IEEE Trans. Power Syst.*, vol. 30, no. 1, pp. 365–375, Jan. 2015.

[16] J. Franco, M. Rider, and R. Romero, "A mixed-integer linear programming model for the electric vehicle charging coordination problem in unbalanced electrical distribution systems," *IEEE Trans. Smart Grid*, vol. 6, no. 5, pp. 2200–2210, Sep. 2015.

[17] G. Benetti, M. Delfanti, T. Facchinetti, D. Falabretti, and M. Merlo, "Real-time modeling and control of electric vehicles charging processes," *IEEE Trans. Smart Grid*, vol. 6, no. 3, pp. 1375–1385, May 2015.

[18] N. Chen, C. W. Tan, and T. Quek, "Electric vehicle charging in smart grid: Optimality and valley-filling algorithms," *IEEE J. Sel. Topics Signal Process.*, vol. 8, no. 6, pp. 1073–1083, Dec. 2014.

[19] M. Jaggi, "Revisiting Frank-Wolfe: Projection-free sparse convex optimization," in *Proc. Int. Conf. Mach. Learn.*, Atlanta, GA, USA, Jun. 2013, pp. 427–435.

[20] S. Boyd and L. Vandenberghe, *Convex Optimization*. New York, NY, USA: Cambridge Univ. Press, 2004.

[21] D. E. Knuth, *The Art of Computer Programming: Sorting and Searching*, vol. 3. Boston, MA, USA: Pearson Education, 1998.

[22] D. P. Bertsekas, *Convex Optimization Algorithms*. Belmont, MA, USA: Athena Scientific, 2015.
[23] L. Gan and S. H. Low, "Convex relaxations and linear approximation for optimal power flow in multiphase radial networks," in *Proc. Power Syst. Comput. Conf.*, Wroclaw, Poland, Aug. 2014, pp. 1–9.
[24] E. Dall'Anese, H. Zhu, and G. B. Giannakis, "Distributed optimal power flow for smart microgrids," *IEEE Trans. Smart Grid*, vol. 4, no. 3, pp. 1464–1475, Sep. 2013.
[25] V. Kekatos, L. Zhang, G. B. Giannakis, and R. Baldick, "Voltage regulation algorithms for multiphase power distribution grids," *IEEE Trans. Power Syst.*, to be published.
[26] S. Boyd, N. Parikh, E. Chu, B. Peleato, and J. Eckstein, "Distributed optimization and statistical learning via the alternating direction method of multipliers," *Found. Trends Mach. Learn.*, vol. 3, pp. 1–122, 2010.
[27] V. Kekatos and G. B. Giannakis, "Distributed robust power system state estimation," *IEEE Trans. Power Syst.*, vol. 28, no. 2, pp. 1617–1626, May 2013.
[28] Q. Peng and S. Low, "Distributed algorithm for optimal power flow on a radial network," in *Proc. IEEE Conf. Decision Control*, Venice, Italy, Dec. 2014, pp. 167–172.
[29] National Household Travel Survey. US Department of Transportation. (2009). [Online]. Available: http://nhts.ornl.gov/2009/ pub/stt.pdf
[30] K. Qian, C. Zhou, M. Allan, and Y. Yuan, "Modeling of load demand due to EV battery charging in distribution systems," *IEEE Trans. Power Syst.*, vol. 26, no. 2, pp. 802–810, May 2011.
[31] Distribution test feeders. IEEE Power & Energy Society. (2013). [Online]. Available: http://ewh.ieee.org/soc/pes/dsacom/testfeeders/index.html
[32] W. H. Kersting, *Distribution System Modeling and Analysis*. Boca Raton, FL, USA: CRC Press, 2002.

Liang Zhang (S'13) received the Diploma, B.Sc., and M.Sc. degrees in electrical engineering from Shanghai Jiao Tong University, Shanghai, China, in 2012 and 2014, respectively. Since then, he has been working toward the Ph.D. degree in the Department of ECE, University of Minnesota, Minneapolis, MN, USA. His current research interests span the areas of optimization, monitoring, and inference for power systems.

Vassilis Kekatos (M'10) received the Diploma, M.Sc., and Ph.D. degrees in computer science and engineering from the University of Patras, Patras, Greece, in 2001, 2003, and 2007, respectively. During the summer of 2012, he worked for Windlogics Inc. After that, he was a Research Associate with the Department of Electrical and Computer Engineering, University of Minnesota. During 2014, he stayed with the University of Texas at Austin and the Ohio State University as a Visiting Researcher, and he received the postdoctoral career development award (honorable mention) by the University of Minnesota. In August 2015, he joined the Bradley Department of Electrical and Computer Engineering of Virginia Tech as an Assistant Professor. His research focus is on optimization, learning, and management of future energy systems. He received the Marie Curie Fellowship during 2009–2012.

Georgios B. Giannakis (F'97) received his Diploma in Electrical Engr. from the Ntl. Tech. Univ. of Athens, Greece, 1981. From 1982 to 1986 he was with the Univ. of Southern California (USC), where he received his MSc. in Electrical Engineering, 1983, MSc. in Mathematics, 1986, and Ph.D. in Electrical Engr., 1986. He was with the University of Virginia from 1987 to 1998, and since 1999 he has been a professor with the Univ. of Minnesota, where he holds an Endowed Chair in Wireless Telecommunications, a University of Minnesota McKnight Presidential Chair in ECE, and serves as director of the Digital Technology Center.

His general interests span the areas of communications, networking and statistical signal processing - subjects on which he has published more than 390 journal papers, 670 conference papers, 25 book chapters, two edited books and two research monographs (h-index 118). Current research focuses on learning from Big Data, wireless cognitive radios, and network science with applications to social, brain, and power networks with renewables. He is the (co-) inventor of 28 patents issued, and the (co-) recipient of 8 best paper awards from the IEEE Signal Processing (SP) and Communications Societies, including the G. Marconi Prize Paper Award in Wireless Communications. He also received Technical Achievement Awards from the SP Society (2000), from EURASIP (2005), a Young Faculty Teaching Award, the G. W. Taylor Award for Distinguished Research from the University of Minnesota, and the IEEE Fourier Technical Field Award (2015). He is a Fellow of EURASIP, and has served the IEEE in a number of posts, including that of a Distinguished Lecturer for the IEEE-SP Society.